Intercalibration of AMSR2 NASA Team 2 Algorithm Sea Ice Concentrations With AMSR-E Slow Rotation Data

Walter N. Meier and Alvro Ivanoff

***Abstract*—Sea ice estimates from AMSR2 are intercalibrated with AMSR-E fields through a two-step process. First, slow rotation 2 r/min AMSR-E data is used to derive regression equations from colocated pairs of AMSR2 and AMSR-E brightness temperatures (T_bs). The regression equations are used to modify AMSR2 T_bs into AMSR-E equivalent T_bs that are then input into the NASA Team 2 (NT2) sea ice concentration algorithm used for the AMSR-E standard products. The regressed T_bs result in changes in sea ice concentration of a few percent compared to using the original un-regressed AMSR2 T_bs. Next, sea ice estimates from the F17 SSMIS sensor are used as a bridge to compare AMSR-E total sea ice extent estimates in 2010 with AMSR2 total sea ice extent estimates in 2013. Based on this comparison, a further adjustment is made to a weather filter threshold used in the NT2 algorithm to minimize the total extent bias between AMSR2 and AMSR-E using a double-differencing approach. The adjustments reduced apparent bias with AMSR-E from ∼200 000 km^2 for the original unmodified AMSR2 T_bs to –700 and 4700 km^2 for the Arctic and Antarctic, respectively. These differences are within the range of previous passive microwave sea ice intercalibrations. The adjusted AMSR2 sea ice fields provide a nearly 15-year time series of sea ice change; depending on the lifetime of AMSR2 and possible follow-on sensors, AMSR2 has the potential to be part of a multidecadal record of sea ice change.**

***Index Terms*—AMSR2, antarctic, arctic, passive microwave (PM), remote sensing, sea ice.**

I. Introduction

ARCTIC sea ice is one of the most iconic indicators of climate change. Several studies have noted significant decreasing trends in sea ice extent over the past 35+ years in all seasons and nearly all regions, e.g., [1], [2]. These long-term time series of sea ice area and extent have been primarily produced from passive microwave (PM) imagery because it provides complete coverage under all-sky conditions. It also enables a long time series because satellite-borne PM sensors have been continuously operating since late 1978.

Manuscript received November 23, 2016; revised April 21, 2017; accepted June 10, 2017. Date of publication July 10, 2017; date of current version September 20, 2017. This work was supported by the NASA as part of the NASA AMSR2 Science Team. *(Corresponding Author: Walter N. Meier.)*

W. N. Meier is with the NASA Goddard Space Flight Center Cryospheric Science Laboratory, Greenbelt, MD 20771 USA (e-mail: walt.meier@nasa.gov).

A. Ivanov is with the NASA Goddard Space Flight Center Cryospheric Science Laboratory, Greenbelt, MD 20771 USA, and also with ADNET Systems, Inc., Bethesda, MD 20817 USA (e-mail: alvaro.ivanoff@nasa.gov).

Digital Object Identifier 10.1109/JSTARS.2017.2719624

The backbone of the PM sea ice record is the series of special sensor microwave imager (SSMI) and special sensor microwave imager/sounder (SSMIS) instruments on U.S. Defense Meteorological Satellite Program (DMSP) platforms that began operating in 1987. Previously, the Scanning Multichannel Microwave Radiometer (SMMR) on the NASA Nimbus-7 platform was in operation, extending the record back to October 1978. To create a consistent time series across the series of instruments, the data must be intercalibrated. This is done by using overlap periods of the sensor missions–i.e., when both old and new sensors are operating–to adjust the data so that the newer sensor's sea ice estimates are consistent with the older sensor's estimates. This has generally been done using daily gridded fields of sea ice concentration for the Arctic and Antarctic. The approaches have generally focused on minimizing differences in total sea ice extent and/or area because these time series are key indicators of climate change and there is the desire to have high confidence in the long-term trend estimates.

More recently, the Advanced Microwave Scanning Radiometer for the Earth Observing System (AMSR-E) on NASA's Aqua satellite operated from June 18, 2002 until October 4, 2011 when the instrument stopped rotating. The Japanese Aerospace Exploration Agency (JAXA) launched a follow-on sensor, AMSR2, on the Global Change Observation Mission 1st–Water (GCOM-W1), but unfortunately, the GCOM-W1 launch on May 18, 2012 was over six months after the AMSR-E ceased fully functioning. This did not allow us to use a standard intercalibration approach of comparing fields between the older sensor and newer sensor because both sensors were not simultaneously operating. Later, the AMSR-E instrument was restarted with a slow rotation (2 r/min compared to a nominal 40 r/min) to provide limited overlap data for intercalibration with AMSR2. With only the fields from AMSR-E 2 r/min data available to compare with AMSR2, the concentration comparisons would be sparse, and total extent and area comparisons would not be feasible.

In this paper, we present the approach used to employ the AMSR-E 2 rpm data to intercalibrate the NASA Team 2 (NT2) algorithm sea ice concentration product from AMSR2 with the NASA AMSR-E standard NT2 product. Assessment of the intercalibration was done via a double-differencing method using SSMIS sea ice fields as a bridge between the AMSR sensors and further adjustments were made to optimize the consistency of total sea ice extent.

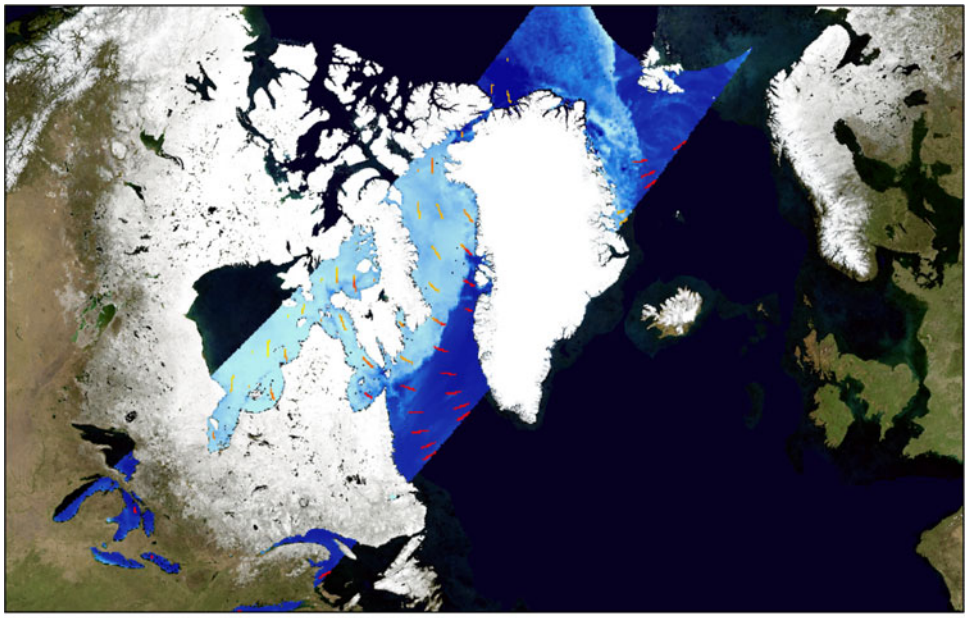

(a)

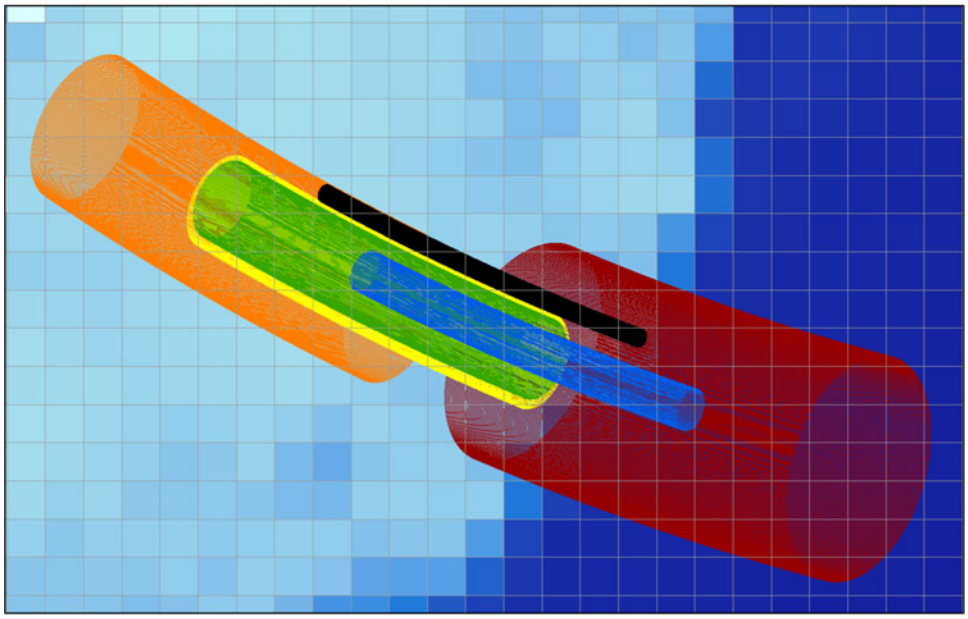

(b)

Fig. 1. Schematic of AMSR-E 2 r/min coverage versus AMSR2. (a) Background swath of AMSR2 89 GHz polarization ratio (PR89) for January 1, 2013 overlaid with AMSR-E 2 r/min coverage in red, orange, and yellow. (b) Close-up schematic of a single 2 r/min scan for each of channel footprints: 6.9 GHz (red), 10.7 GHz (orange), 18.7 GHz (yellow), 23 GHz (green), 36.5 GHz (blue), and 89 GHz (black); the background image is an AMSR2 PR89 partial swath on the 12.5 km polar stereographic grid.

II. Data

For this study, AMSR2 and AMSR-E brightness temperatures (T_bs) were acquired from JAXA. For AMSR-E, we obtained the Level 1S slow-rotation 2 r/min T_bs for the calendar year 2013 [3]. The slow rotation means that a normal scan line is compressed along the scan, leading to scattered short "dashes" of scans in each swath (see Fig. 1). In other words, the footprints in the 2 r/min fields have far more overlap and cover a distance much shorter than the standard 40 r/min scan line. Since the issue with AMSR-E was the rotation and not the sensor itself, we assume that the 2 r/min T_bs are of consistent quality with the 40 r/min field from earlier, though the slower rotation may have some impact (for example on hot and cold load calibration), but the effects appear to be minimal.

For AMSR2, we obtained Level 1R (L1R) Version 1 T_bs [4] at the 23 GHz footprint resolution (15 $\times$ 26 km). The AMSR2 T_bs and 2 r/min AMSR-E T_bs swaths were each gridded onto a 12.5 km polar stereographic grid for both the Arctic and Antarctic regions using a drop-in-the-bucket approach. Because of the slow rotation, there were many more footprints in each grid

where the AMSR-E 1S had data than in the nominally rotating AMSR2. All footprints that had their center within a grid cell were averaged for each sensor. We also note that due to resolution and scan angle differences, different channels of the 2 r/min data are not colocated [see Fig. 1(b)]. So the scan lines of each channel were gridded separately at their specific locations. The end result is a set of colocated gridded swath fields for each sensor and each channel used in the NT2 algorithm (18–89 GHz) of each sensor. AMSR2 and AMSR-E are both in the "A-Train" orbit (an AM pass orbit with several satellites) and their observation times were different by just a few minutes. So the colocated set of AMSR-E and AMSR2 2 r/min $\mathrm{T_b}$ fields were nearly coincident in time as well. The resulting set of value pairs from the common grid cells were used to derive the linear regression coefficients for each channel in the equations discussed below.

The full AMSR2 L1R fields were input into the NT2 algorithm (described below) to produce hemispheric daily average sea ice concentration estimates gridded onto a 12.5 km resolution polar stereographic grid. AMSR-E sea ice concentrations were obtained from the National Snow and Ice Data Center (NSIDC) [5] for 2010 and 2011; these are also a daily gridded product on the 12.5 km polar stereographic grid. For intercomparison between the AMSR products, SSMIS NASA Team Sea Ice Concentrations [6] were also obtained, for the period 2010–2013; the data are daily averages on a 25 km polar stereographic grid.

III. Algorithm Description

There are several sea ice algorithms to derive concentration from input PM brightness temperature data. The different algorithms use different approaches and different combinations of channels, which lead to different sensitivities to surface and atmospheric conditions [7], [8]. Here we focus on the NT2 algorithm [9], [10], because it is the standard algorithm for the NASA AMSR-E sea ice concentration product. Most PM algorithms are empirically derived using a combination (differences and/or ratios) of channels (frequency/polarization). Coefficients or "tie points" are derived for three (two sea ice, one water) pure surface types based on the $\mathrm{T_b}$ distributions, and concentration is estimated based on linear interpolation of the channel differences/ratios between the tie points of the pure surface types.

The NT2 algorithm is formulated differently than other PM sea ice concentration algorithms in several ways. One difference between NT2 and many other algorithms is that, in addition to 19 and 36 GHz frequencies, NT2 employs high frequency 89 GHz channels. However, the atmosphere significantly influences the 89 GHz channels. To address this, an inverse atmospheric radiative transfer model is employed to provide an atmospheric correction. Another difference is that while some algorithms are applied to gridded daily average $\mathrm{T_b}$s, the NT2 is run on swath $\mathrm{T_b}$s and, then an average gridded concentration field is produced from the swath concentrations.

The algorithm utilizes an iterative scheme that fits a model to observed $\mathrm{T_b}$ ratios. The model is effectively a look-up table of $\mathrm{T_b}$s corresponding to two $\mathrm{T_b}$ ratios for concentrations between 0% and 100% for 12 standard atmospheres, resulting in a $12 \times 101 \times 101$ matrix of model concentrations. The look-up table values were derived from atmospheric station data and a radiative transfer model. For each swath footprint, the concentration is estimated by iterating through a cost function based on the difference between observed $\mathrm{T_b}$ ratios and the modeled ratios. The final estimated concentration is the model concentration value that minimizes the cost function.

After concentration is retrieved a further screening is performed on each swath to remove potential weather effects. While the open ocean generally has a distinct microwave signature than that of sea ice, the presence of thick clouds, precipitation, or wind roughening of the surface can result in false ice detection by the algorithm. These effects can largely be screened out with the use of gradient ratio thresholds [10], [11]. The gradient ratio weather filters used for this purpose are derived from the 18, 23, and 36 GHz vertically polarized channels:

$$GR_{3618} = \frac{(T_b 36\ \mathrm{V} - T_b 18\ \mathrm{V})}{(T_b 36\ \mathrm{V} + T_b 18\ \mathrm{V})} > 0.05 \tag{1}$$

$$GR_{2318} = \frac{(T_b 23\ \mathrm{V} - T_b 18\ \mathrm{V})}{(T_b 23\ \mathrm{V} + T_b 18\ \mathrm{V})} > 0.045. \tag{2}$$

If either GR value exceeds the threshold, the sea ice concentration in that grid cell is set to 0. While the motivation of the GR thresholds is primarily to remove weather effects, they also have the effect of eliminating most low concentration retrievals below $\sim$15%. This means that to some degree, applying the GR filters defines the ice edge at $\sim$15%, which corresponds to the definition used by many PM sea ice products [e.g., 12]. Final postprocessing steps are then done to minimize erroneous retrievals, including screening out grid cells potentially affected by land-spillover effects (mixed land-ocean grid cells) [10]. Such quality control steps do not completely remove errors and do not address other known issues with PM sea ice data, including seasonal melting, biases from melt ponds, freeze-up effects, and thin ice biases.

IV. Intercalibration Approach

Intercalibration between sensors is traditionally done by comparing their colocated data during their overlapping operational periods. An adjustment is made to one (or both) of the sensors to optimize the match between them. This allows us the data from the series of sensors to be "stitched" together to form a unified time series.

For sea ice, this has typically been done by adjusting algorithm coefficients, or tie points, that correspond to the pure surface types for each of the channels [12], though more recently dynamic tie-point approaches have been implemented, where tiepoints are derived on-the-fly based on the same $\mathrm{T_b}$ data used to derive the concentration [e.g., 8]. The tie points are adjusted for the new sensor based on a linear regression of $\mathrm{T_b}$s between the two sensors. The objective is to have consistency in the algorithm outputs of concentration, extent, and area. Extent and area are of particular focus because these are used as important indicators of climate change. In some cases, further tie point adjustments are made to optimize the match in extent

and/or area (i.e., minimize the difference in the value between the sensors) [12]. This further optimization is likely needed for two reasons. First, the regressions have been conducted on gridded daily average T_bs; different sensors will have at least slightly different orbits and thus different overpass times; this means that rapidly changing atmospheric (e.g., water vapor, liquid water) and surface properties (e.g., surface melt) may affect the detected T_bs between two overpass times. Second, some of the sensor overlap periods have been quite short in the PM sea ice record–as little as a few weeks; particularly at certain times of year (especially summer) when surface variability is high, a simple brightness temperature regression may not be able to fully minimize differences between sensor outputs. Ideally, at least a full year is needed to fully encompass all seasonal variability in both hemispheres [13]. In addition, for some overlaps, further adjustments are done to the GR weather filter ratios to eliminate false weather signals and optimize the match between sensor outputs [14].

For the AMSR2 NT2 product, a different approach is needed because there is no sensor overlap between the fully functioning AMSR-E and AMSR2. The only overlap is with AMSR-E at 2 r/min. Regressions can be run with the more limited brightness temperature sample, but total extents and areas cannot be compared to assess overall consistency of the sea ice product. Our approach is two-pronged: 1) derive regression coefficients based on the overlap with the 2 r/min AMSR-E data, and 2) assesses consistency and make further needed adjustments based on a cross-comparison with sea ice fields from the DMSP SSMIS sensor.

A. Regression of AMSR2 With 2 r/min AMSR-E

A full year of 2 r/min AMSR-E data was acquired for the calendar year 2013. Daily brightness temperature regressions were calculated for each of the channels used by NT2 (18.7–89.0 GHz). The regressions were limited to regions of sea ice and ocean near the ice edge. This approach restricts the regressions to only regions that are directly relevant to the sea ice product and avoids potential noise or biases that may be introduced from land and tropical ocean regions. Separate regressions were done for each hemisphere, as in previous approaches [11]–[13].

Because of the slow rotation, the 2 r/min AMSR-E footprints are squeezed together along the swath line and thus cover a narrower region across the swath than the full rotation speed 40 r/min AMSR2 footprints. In addition, the 2 r/min swaths are spread out along the orbital track with large gaps along-track between swaths; this is in contrast to the 40 r/min data where the rotation is fast enough for swaths to slightly overlap along-track and not leave any gaps. To address this inconsistency, only 40 r/min AMSR2 footprints that were colocated with the sparser AMSR-E footprints were sampled to obtain a set of "pseudo-2 rpm" AMSR2 footprints for each swath gridded onto the polar stereographic grid.

Using these sets of 2 r/min footprints, linear regressions were computed from all colocated points from all swaths for each day. The number colocated points varied depending on the time of year (ice and near-ice regions), with 15 000 to 25 000 points total from the swaths each day. There are two possible approaches to the regression. One approach that has been typically employed in the past [e.g., 12] is to use the regression to adjust the algorithm coefficients (tie points) used for the older sensor to the newer sensor. In this approach, the T_bs from the new sensor are unchanged and the adjusted tie points correct for the differences between the sensors. Because the NT2 algorithm has 12 different atmospheres, it effectively has 12 sets of tie points for each of the three surface types and the seven channels [10]. In addition, these tie points were derived using an outdated and now unavailable radiative transfer model. Thus, this method would requirement implementation of a new radiative transfer model. This would be time-consuming. In addition, the old model was employed for AMSR-E and continuity, any new model would need to be implemented for the AMSR-E products, which is beyond the scope of this project. Instead we employed the alternative approach of using the regression to adjust AMSR2 T_b retrievals to match AMSR-E T_bs. In effect, the regression equations were applied to AMSR2 T_bs to create equivalent AMSR-E T_bs that could use the same AMSR-E tie points, as given by:

$$T_b\left(\mathrm{AMSRE}_{\mathrm{equivalent}}\right) = m(T_b\left[\mathrm{AMSR2}\right]) + b \qquad (3)$$

where m is the slope of the linear regression and b is the intercept. Regressions were run for each day and slope and intercepts were calculated. The daily slope and intercept values were averaged over a month and a set of 12 monthly slope and intercepts were calculated for each hemisphere.

We found the slope and intercept values were reasonably consistent in each of the months (see Fig. 2), so for simplicity we averaged the 12 monthly values into a single set of regression coefficients for each channel and these were chosen as the final values used in the algorithm (see Table I). The regressions show a very close agreement between AMSR-E and AMSR2 with correlations >0.99 except for the 89 GHz channel, which are slightly lower due to greater atmospheric influence at the high frequency. Most slopes are near 1 and most intercepts are <5 K. The exception is the 18 V channel, whose slope is noticeably higher than the other channels and whose intercept is $\sim$10 K. It is not clear why the 18 V channel has a larger difference, but it may be related to effects of sensor design and/or onboard calibration (hot load and cold sky calibration targets). Another feature of the regression is that the Arctic and Antarctic regression coefficients are quite similar, including the 18 V channel being an outlier. The overall close match between the sensors is not surprising given the similarity in orbits and in sensor design (similar sensor footprints) and provides confidence that the AMSR2 sensor can provide high consistency with AMSR-E for sea ice products.

Since the correlations are so high, it is not surprising that the regression adjustment to the AMSR2 T_bs yields generally small differences in concentration, generally just a few percent (see Fig. 3), though near the ice edge a few differences are 10% or higher. The ice edge is where the surface is most variable, so differences are expected to be higher there. In addition, the larger 18 V regression coefficients may have an effect because of greater sensitivity at 18 GHz to thin and/or low concentration ice. However, because there is no full AMSR-E overlap field with which to compare, we cannot assess the degree of agreement

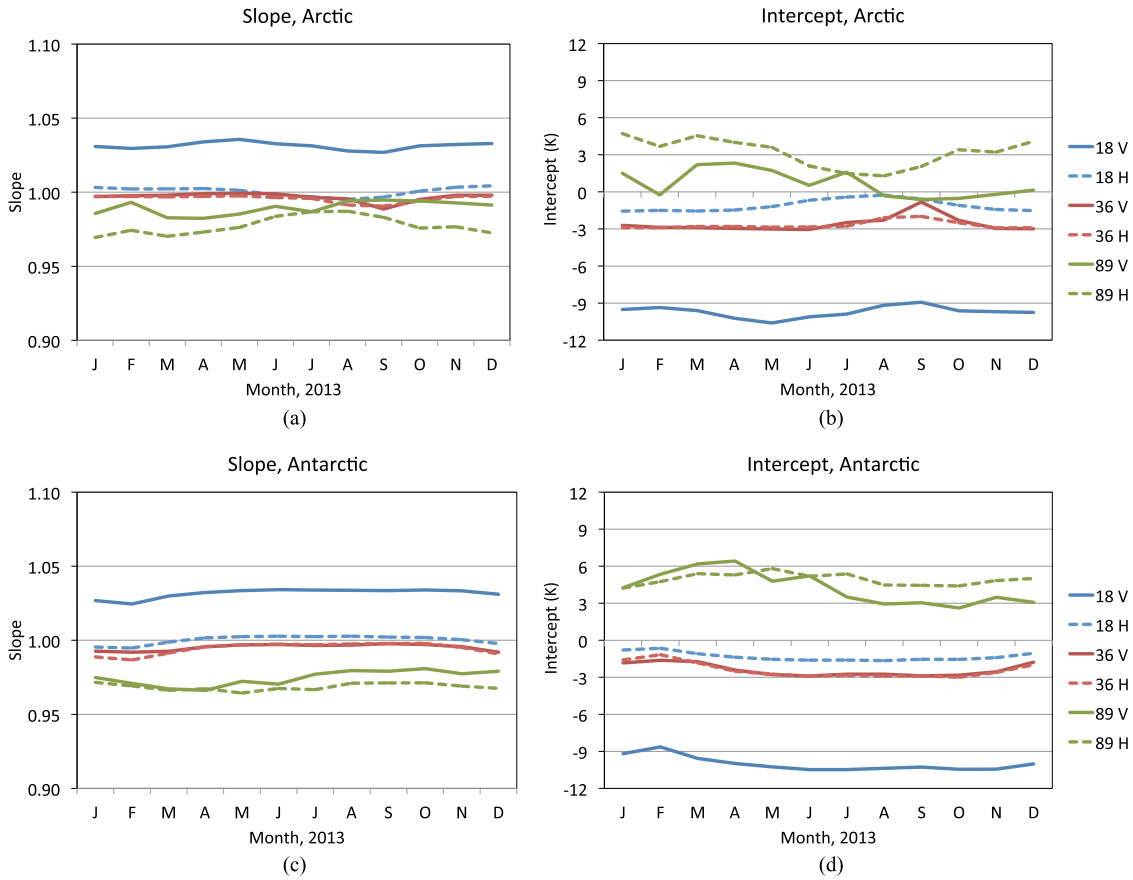

Fig. 2. Monthly regression coefficients for AMSR2 and 2 r/min AMSR-E for 2013. Arctic (a) slope and (b) intercept, and Antarctic (c) slope and (d) intercept for the 18, 36, and 89 GHz channels used in the NT2 algorithm.

TABLE I
AVERAGE REGRESSION AND CORRELATION COEFFICIENTS FOR AMSR2 T_B S, BASED ON COMPARISON WITH 2 R/MIN AMSR-E T_B S FOR JANUARY–DECEMBER 2013

	Northern Hemisphere			Southern Hemisphere		
Channel	Slope	Intercept	Correlation	Slope	Intercept	Correlation
18 V	1.031	–9.710	0.9984	1.032	–10.013	0.9982
18 H	1.001	–1.104	0.9985	1.000	–1.320	0.9983
23 V	0.999	–1.706	0.9979	0.993	–0.987	0.9976
36 V	0.997	–2.610	0.9916	0.995	–2.400	0.9919
36 H	0.996	–2.687	0.9938	0.994	–2.415	0.9932
89 V	0.989	0.677	0.9766	0.975	4.239	0.9619
89 H	0.977	3.184	0.9621	0.969	4.935	0.9549

between the AMSR2 and AMSR-E over complete fields. We need another approach to assess the consistency between the sea ice estimates from the two sensors.

B. Comparison With SSMIS and Further Adjustments

Typically, the regressions are evaluated via hemispheric comparison of total extent and/or area estimates derived from the sea ice concentration algorithm [e.g., 12–14]. Depending on how close the values agree, further adjustments to either the tie points or the gradient ratio weather thresholds may be needed to minimize biases in extent and/or area. Optimizing for hemispheric agreement may come at the expense of optimal agreement in a specific region, however. Ideally, for regional studies, intercalibration would be optimized for the specific region. Here our focus is on hemispheric sea ice properties. In addition, it is not necessarily possible to optimize agreement of both extent and area because extent is most sensitive to the ice edge where concentration is low and area changes would be small, as is discussed below.

Regardless, a full hemispheric (or even region) comparison of extent or area is not possible with the sparse 2 r/min AMSR-E data. Instead, we use a "bridge" data set to cross-compare total extent between AMSR-E and AMSR2 when each were fully functional. The bridge data set is the NASA Team product from the DMSP SSMIS sensor, produced by NASA Goddard and archived at NSIDC [6] for 2011 through 2013. This is the original NASA Team algorithm, a more basic formulation than NT2 that does not use the high frequency 89 GHz channels, nor tabulated radiative transfer model outputs [6], [12], [15]. NT2 was not implemented for SSMIS because coefficients have not been derived for the SSMIS sensor and deriving them would require yet another regression and require the radiative transfer model. The different algorithm and the different sensor means that the NT product produces considerably different sea ice estimates than the AMSR2 and AMSR-E NT2 fields. In addition

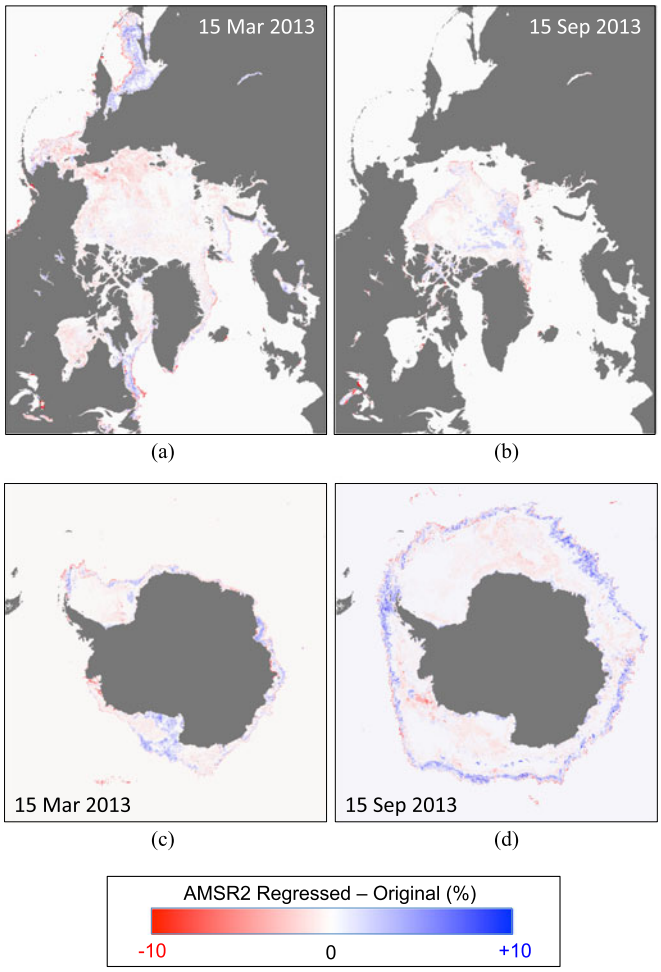

Fig. 3. AMSR2 concentration differences for NT2 output using regressed T_bs and the original T_bs. Examples provided for (a) Arctic March, (b) Arctic September, (c) Antarctic March, and (d) Antarctic September.

the sensor resolution is substantially different between SSMIS and AMSR, and the gridded resolution of the datasets used is also different –25 km for SSMIS versus 12.5 km for AMSR. These differences, in addition to affecting the detection of the ice edge, also result in differing impacts of land-spillover. All of these effects mean that the SSMIS retrievals are not consistent with AMSR. However, here we use the SSMIS total extent fields only as a reference baseline, so the absolute extent differences are not important as long as the SSMIS product is stable, i.e., that there is no artificial trend introduced due to instrument changes such as sensor drift or a switch in sensors. The SSMIS NASA Team fields are consistently produced and for the period analyzed use only the SSMIS on the DMSP F17 platform, so there are no sensor intercalibration issues. Sensor drift could be a concern, but it should be small over just a three-year interval. This means that the SSMIS NASA Team fields should be consistent over the period of interest and can be used as a stable baseline with which to intercompare AMSR-E and AMSR2 sea ice estimates.

The approach is to difference AMSR-E and SSMIS extent during the 2010 overlap and AMSR2 and SSMIS during the 2013 overlap, providing a full one calendar-year period for both sensors. For consistency, the extent calculations assume that the missing data region near the pole (the "pole hole") is ice-covered in all data sets. Retrievals from lakes are not included in the extent estimates. The same foundational land masks were used for all three products, but the masks are resolution dependent, meaning that the SSMIS mask is in practice slightly different. However, the masks are consistent over the time period, so any differences result in an offset with SSMIS that is the same for AMSR2 and AMSR-E. If AMSR-E and AMSR are consistent, then on average the difference with SSMIS should be the same. This can be directly quantified via a double differencing: subtracting the AMSR-E–SSMIS extent from the AMSR2–SSMIS extent. This effectively yields a direct difference of AMSR2–ASMR-E. Of course, AMSR2 and AMSR-E are from different years, so there will be variation in specific conditions, such as the extent and concentration of the ice, the size and location of the marginal ice zone, the timing of melt and freeze-up, and the atmospheric conditions through the two different years. However, over a year the difference should provide an indication of the consistency between AMSR2 and AMSR-E sea ice extents.

Comparing the AMSR-E, AMSR2, and SSMIS total extent time series, there is a fairly close match, but with a noticeable low bias of AMSR-E relative to SSMIS in the Arctic, while the unadjusted (without T_b regression) AMSR2 has a slight high bias (see Fig. 4). In the Antarctic, the bias changes seasonally, with AMSR-E being higher than SSMIS in summer and lower in winter. AMSR2 has the same high summer bias in the Antarctic and near-zero bias during winter. In addition, there are clear spikes in the original AMSR2 extent. These correspond to weather effects that the GR weather filters miss because the T_bs do not have regression coefficients applied. The spikes are more evident in looking at the extent difference time series (see Fig. 5). There is day-to-day variation in the difference and a clear seasonality is seen (likely due to the sensitivity of the algorithms to variations in surface properties such as snow or surface melt, as well as to the different spatial resolution between the sensors). However, the patterns are similar between the two sensor differences except that there is a clear offset between AMSR2 and AMSR-E, with the AMSR2 extent being on average $\sim$200 000 km^2 higher than AMSR-E relative to SSMIS. The regression clearly brings the AMSR2 minus SSMIS difference more in line with the AMSR-E minus SSMIS difference and reduces the spikes in the difference time series due to weather effects. However, the AMSR2 difference still appears to be overall biased higher than the AMSR-E difference, indicating that the regression does not fully reconcile the two time series.

To understand this difference, further inspection of concentration grids was done, which revealed two issues. First, some weather effects were still making it past the weather filter. Second, there were occasionally small discrepancies at the ice edge–some grid cells would be above the 15% threshold in the field from one sensor but not in the other. In addition to screening out weather, the GR filters effectively set a lower limit on the concentration that can be retrieved of $\sim$15%. So discrepancies in the GR filter output not only potentially allow differing weather

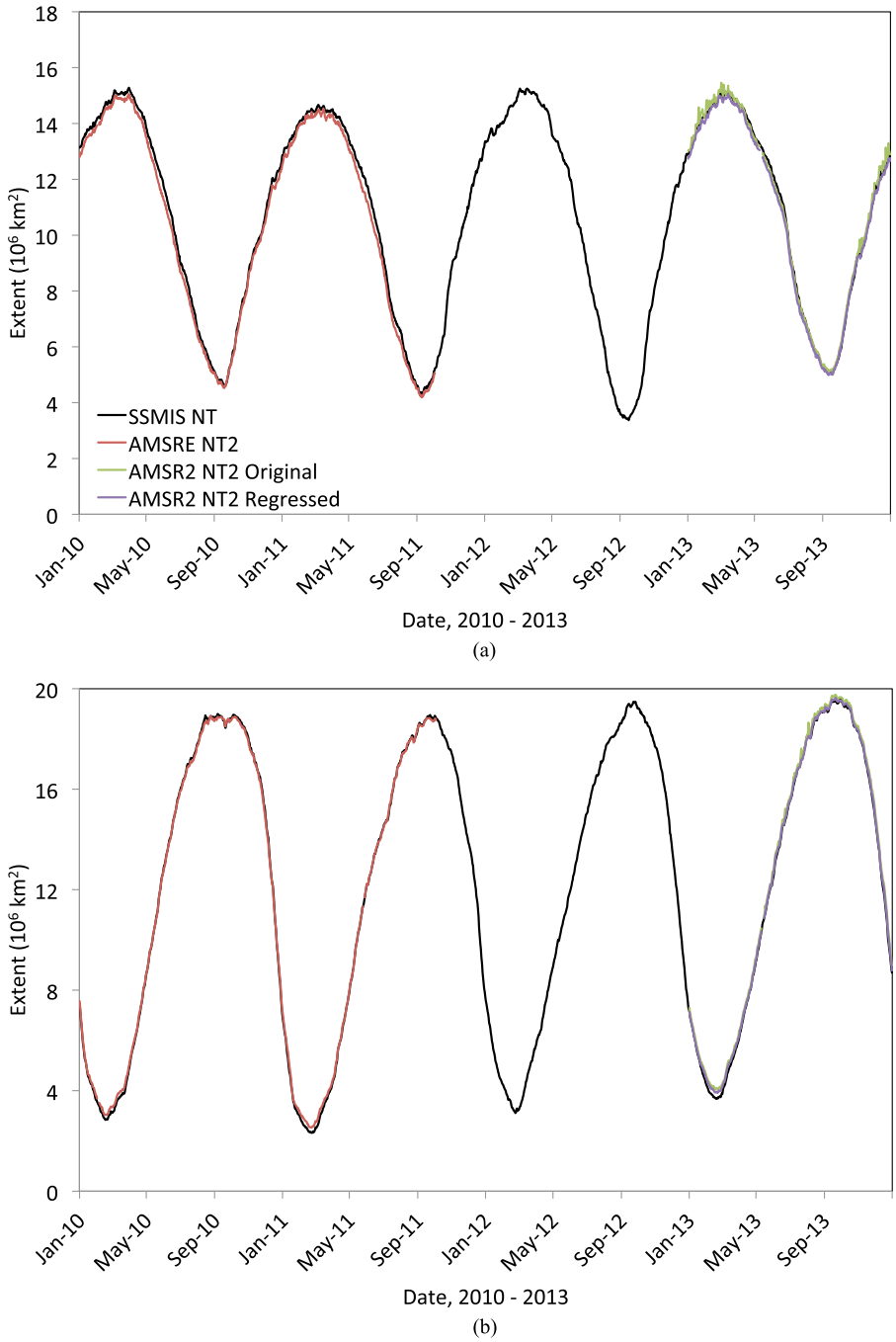

Fig. 4. Total extent time series from January 2010 through December 2013 for (a) Arctic and (b) Antarctic sea ice. AMSR-E data (red) spans January 2010 to October 2011, AMSR2 (original, green, and regressed, purple) spans the calendar year 2013, and SSMIS (black) spans the entire four year period.

effects, but can also result in slightly different ice edges that influence the total extent.

We addressed this by adjusting the GR threshold, as has been done for some previous intercalibrations [12], to reduce the extent bias as much as possible. This was done iteratively, where the full year of concentration fields were processed repeatedly with different GR threshold values. The GR3618 and GR2318 thresholds were each incremented independently by 0.001 and total extents were calculated. Changing the GR2318 threshold was found to have very little effect on the total extent, but modifying the GR3618 threshold did have a noticeable influence. Adjusting the GR3618 threshold from 0.05 to 0.046 yielded the best consistency between AMSR2 and AMSR-E. This is indicated in the time series of double-differenced AMSR2 minus AMSR-E extents, produced by subtracting the AMSR2-SSMIS difference (for 2013) from the AMSRE-SSMIS difference (for 2010), to obtain an effective AMSR2-AMSRE difference (because the SSMIS is canceled out in the double difference) (see Fig. 6). The bias in the Arctic is reduced from over 200 000 km^2 in the original AMSR2 data to only 700 km^2

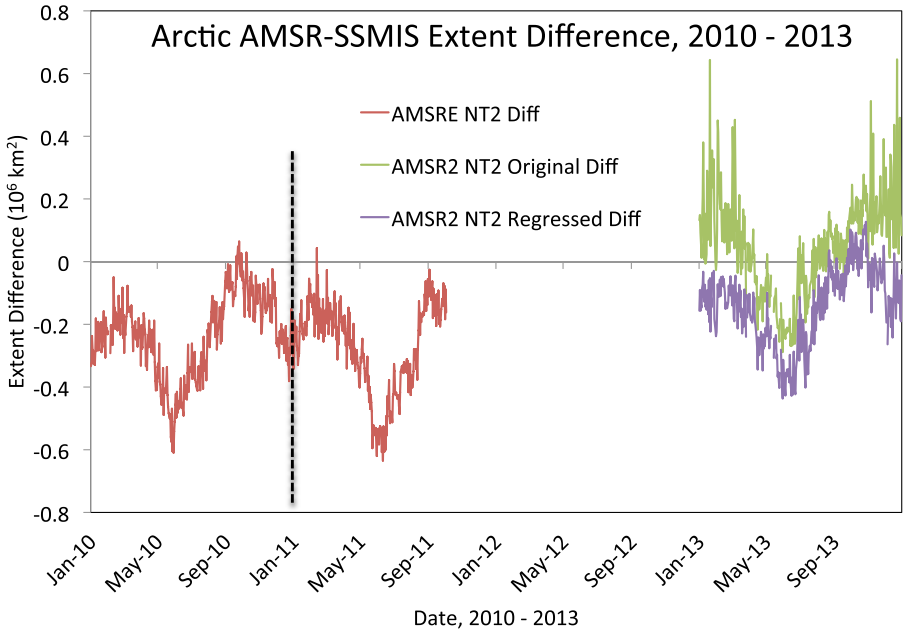

Fig. 5. AMSR minus SSMIS difference for AMSR-E (red), original (green), and regressed (purple) AMSR2 for the Arctic. The dashed line demarcates January 1, 2011. Only the calendar year 2010 data is used for the comparison, but 2011 (up to October) is shown here to demonstrate that there is consistent seasonality in the AMSR-E minus SSMIS difference.

(see Table II), which corresponds to ~4.5 grid cells; the bias in the Antarctic is reduced to 4700 km^2, ~30 grid cells. Both of these biases are as low as or lower than previous inter-sensor calibrations for sea ice products [12]–[14]. We note that because two different years are used, conditions are different, and we cannot have as much confidence as we could with a coincident intersensor calibration. The GR correction may include the influence of variable weather effects and surface properties (e.g., melt, thin ice) between the two years.

Nonetheless, the regression and GR adjustment substantially improved the agreement in total extent. In particular, it largely removes a seasonal effect in the Arctic, with larger differences during the winter, which is likely due to a longer ice edge and the variability of the thin ice near the winter edge. In the Antarctic, the regression and GR adjustment largely remove a trend through the year toward larger differences and more variability. Some periods of higher differences do remain during parts of June, August, November, and December, but overall the bias is lowered to near zero. The effectiveness of the GR adjustment is perhaps not surprising in light of the outlier 18 V regression coefficients compared to the other channels (see Fig. 2, Table I). Since the 18 V channel is a component in both weather filters, the larger discrepancy may explain why the GR adjustment was needed. The consistency could be further investigated by looking at a longer time period, though one year encompasses a full seasonal cycle and thus should capture all types of transitions during the year.

For completeness, we also examined total area using the same double-differencing method. Area is not expected to be as consistent for a couple of reasons. First, we have chosen to optimize the extent agreement, adjusting the GR3618 threshold in order to minimize the difference between AMSR2 and AMSR-E extent relative to SSMIS. This adjustment occurs right near the ice edge, where concentrations are low. Thus, the adjustment will not affect area much.

Second, the SSMIS NT product is known to underestimate concentration depending on conditions, particularly melt. Since we are bridging two different years, the different surface and atmospheric conditions in the two year will have varying effects on the SSMIS area estimates and thus on the double-differencing.

So it is not surprising that the double-difference total area values do not match as well as extent, with differences ~200 000 km^2 (see Table II; Fig. 7). The regression and GR3618 adjustment do not change this much.

V. Summary

We have described here a novel approach to the intercalibration of PM sea ice fields from AMSR2 and AMSR-E where there is not overlap of complete data. We used the limited 2 r/min AMSR-E data to derive the regression coefficients from colocated AMSR2 T_bs. We used the regression coefficients to adjust AMSR2 T_bs to match AMSR-E T_bs. This allowed us to keep the algorithm static with the same algorithm coefficients. SSMIS sea ice fields were then used to evaluate the effectiveness of the regression via a double-differencing to deduce extent biases between AMSR2 and AMSR-E. To reduce that bias as much as possible, iterative adjustments to the GR3618 and GR2318 weather filter thresholds were then made to find the GR thresholds that minimized the bias. This resulted in a change to the GR3618 threshold from 0.050 to 0.046.

Although this approach may not be as optimal as having data from overlapping fully functional sensors, it provides a high-quality intercalibration of extent between AMSR2 and

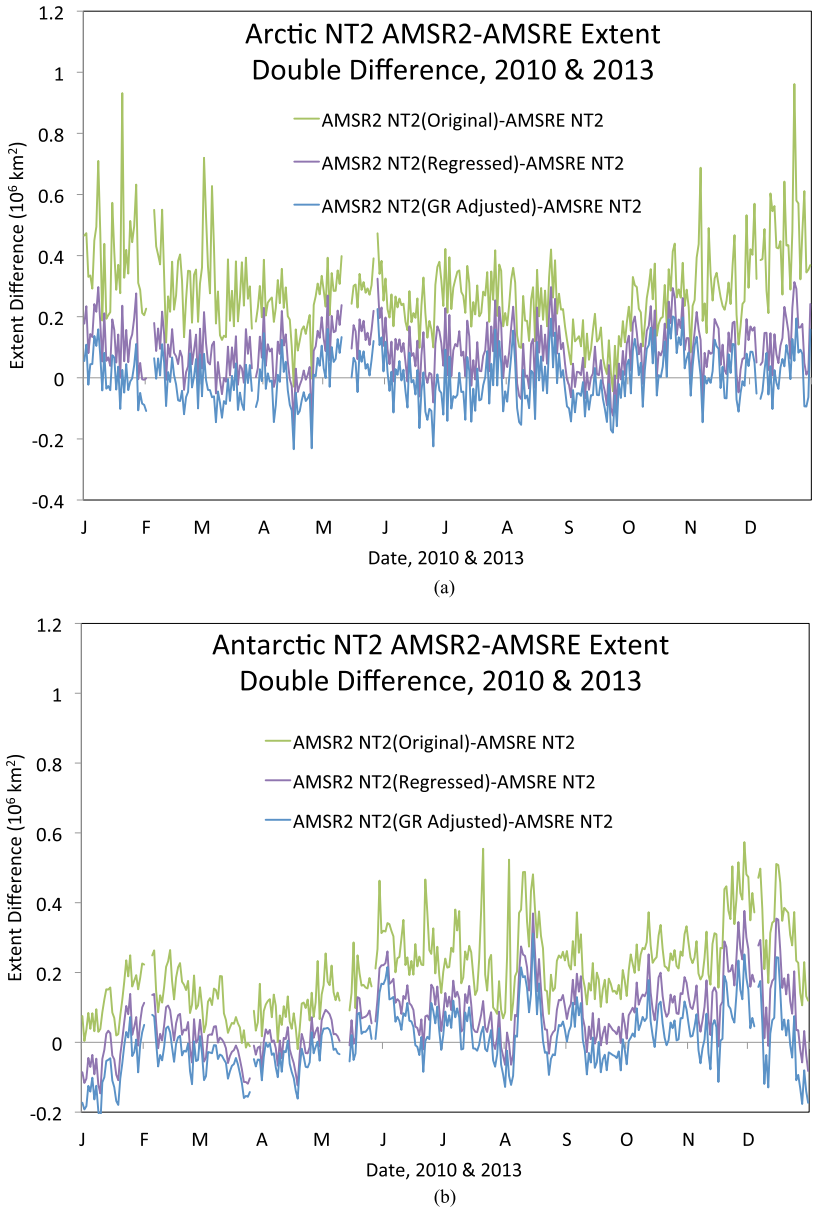

Fig. 6. (a) Arctic and (b) Antarctic extent double differences, (AMSR2–SSMIS)–(AMSR-E–SSMIS) for original AMSR2 (green), regressed AMSR2 (purple), and regressed AMSR2 with GR adjustment (blue).

TABLE II
TOTAL SEA ICE EXTENT AND AREA BIAS AND DIFFERENCE STANDARD DEVIATION (IN PARENTHESES) BETWEEN AMSR2 AND AMSR-E BASED ON DOUBLE-DIFFERENCE WITH SSMIS EXTENT (KM^2)

	Extent		Area	
	Arctic	Antarctic	Arctic	Antarctic
Original AMSR2	282 300 (137 500)	208 200 (117 300)	227 700 (163 300)	242 600 (172 900)
Regressed AMSR2	92 300 (87 800)	71 900 (94 400)	216 500 (174 000)	255 800 (170 600)
GR Adjusted AMSR2	–700 (84,200)	4700 (87 500)	192 600 (173 500)	220 100 (175 200)

AMSR-E. This allows us to provide a consistent AMSR-based extent time series of now nearly 15 years (June 2002 to present, with a gap from October 2011 to August 2012), which will extend for at least as long as AMSR2 is operational (potentially longer if ASMR-like sensors are continued in the future). As we show here, area is not as consistent and the approach has only minimally improved the agreement. This is partly because the comparison SSMIS product is limited for accurate area retrievals, particularly during summer. Also, in the procedure we chose here, we prioritized extent because it is more commonly used for climate trends and is less affected by potential changes in melt and resulting surface effects that may bias area trends. It is likely not possible to optimize both extent and area [13], though a more balanced approach than used here could be implemented. For some applications, area is of more interest, for example examining polynyas in the Antarctic.

NT2 concentration fields and other AMSR2 products are currently in development at NASA and will be distributed by

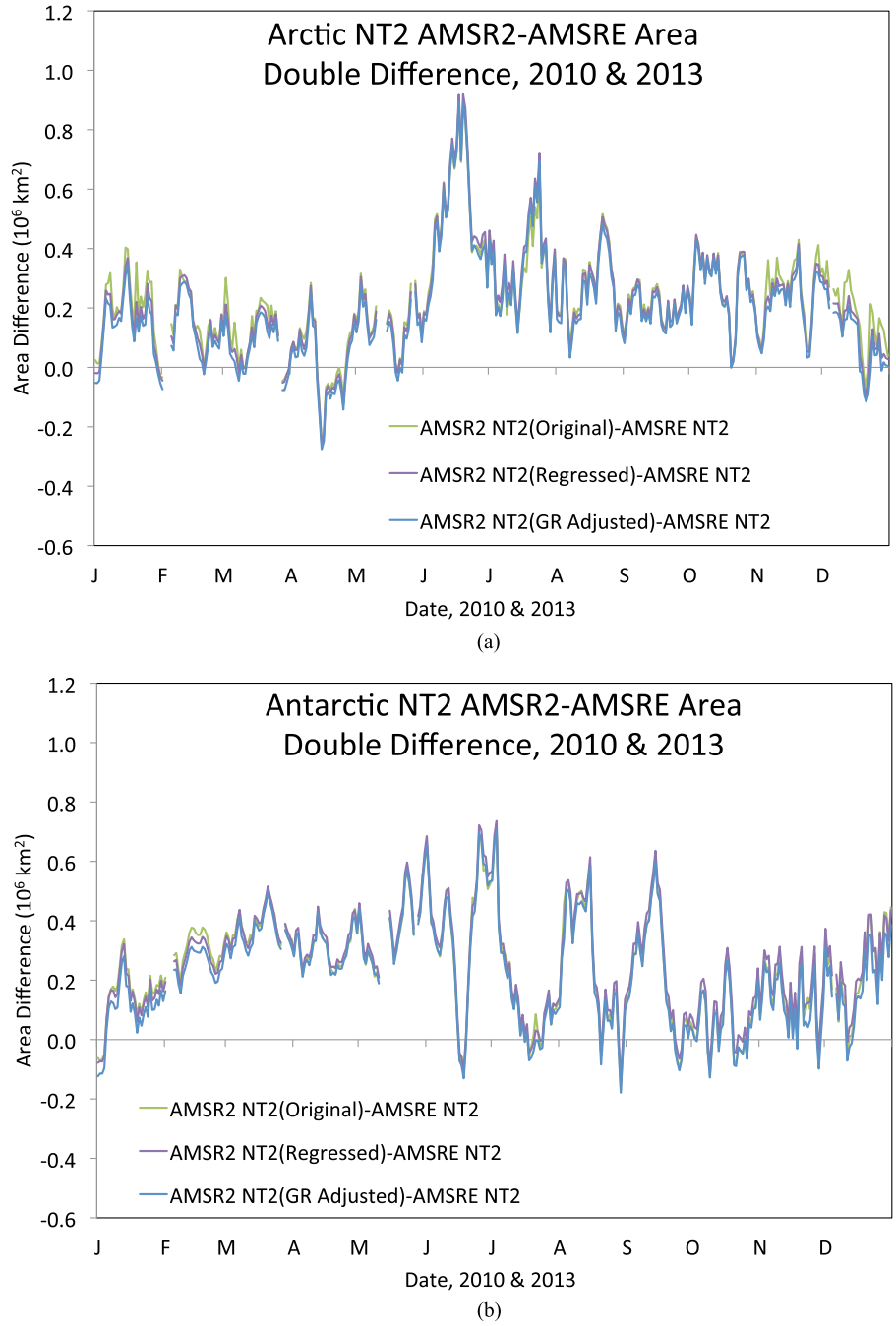

Fig. 7. (a) Arctic and (b) Antarctic area double differences, (AMSR2–SSMIS)–(AMSR-E–SSMIS) for original AMSR2 (green), regressed AMSR2 (purple), and regressed AMSR2 with GR adjustment (blue).

NSIDC. The AMSR record, though shorter than the SMMR-SSMI-SSMIS time series, provides higher spatial resolution and uses the more advanced NT2 algorithm for its standard product. Thus, the intercalibrated AMSR-E and AMSR2 sea ice data has the potential to provide an enhanced consistent multidecadal record of climate change in the Arctic. The approach here could be applied more widely to other past PM sensor transitions through the use of model estimates as the "bridge" between sensors. This would potentially address the limitations due to short sensor overlap periods, such as SMMR and SSMI, and provide a consistent baseline across all sensors.

REFERENCES

[1] W. N. Meier *et al.*, "Arctic sea ice in transformation: A review of recent observed changes and impacts on biology and human activity," *Rev. Geophys.*, vol. 41, pp. 185–217, 2014, doi: 10.1002/2013RG000431.

[2] C. L. Parkinson and N. E. DiGirolamo, "New visualizations highlight new information on the contrasting Arctic and Antarctic sea-ice trends since the late 1970s," *Remote Sens. Environ.*, vol. 183, pp. 198–204, 2016, doi: 10.1016/j.rse.2016.05.020.

[3] *AMSR-E Slow Rotation Data Format Description Document*, Tokyo, Japan: JAXA, 2013, [Online]. Available: http://sharaku.eorc.jaxa.jp/AMSR/products/amsre_slowdata.html

[4] *Data User's Manual for the Advanced Microwave Scanning Radiometer 2 (AMSR2) Onboard the Global Change Observation Mission 1st–Water "Shizuku" (GCOM-W1),* 3rd ed. Tokyo, Japan: JAXA, 2016. [Online]. Available: http://suzaku.eorc.jaxa.jp/GCOM_W/data/data_w_use.html

[5] D. J. Cavalieri, T. Markus, and J. C. Comiso, *AMSR-E/Aqua Daily L3 12.5 km Brightness Temperature, Sea Ice Concentration, & Snow Depth Polar Grids, Version 3*. Boulder, CO, USA: NASA, 2014. [Online]. Available: http://dx.doi.org/10.5067/AMSR-E/AE_SI12.003

[6] D. J. Cavalieri, C. L. Parkinson, P. Gloersen, and H. J. Zwally, *Sea Ice Concentrations from Nimbus-7 SMMR and DMSP SSM/I-SSMIS Passive Microwave Data, Version 1*. Boulder, CO, USA: NASA, 1996. [Online]. Available: http://dx.doi.org/10.5067/8GQ8LZQVL0VL.

[7] N. Ivanova, O. M. Johannessen, L. T. Pedersen, and R. T. Tonboe, "Retrieval of Arctic sea ice parameters by satellite passive microwave sensors: A comparison of eleven sea ice concentration algorithms," *IEEE Trans. Geosci. Remote Sens.*, vol. 52, no. 11, pp. 7233–7246, Nov. 2014.

[8] N. Ivanova *et al.*, "Inter-comparison and evaluation of sea ice algorithms: Towards further identification of challenges and optimal approach using passive microwave observations," *The Cryosphere*, vol. 9, pp. 1797–1817, 2015, doi: 10.594/tc-9-1797-2015.

[9] T. Markus, and D. J. Cavalieri, "An enhancement of the NASA team sea ice algorithm," *IEEE Trans. Geosci. Remote Sens.*, vol. 38, no. 3, pp. 1387–1398, May 2000, doi: 10.1109/36.843033.

[10] T. M. Markus and D. J. Cavalieri, "The AMSR-E NT2 sea ice concentration algorithm: Its basis and implementation," *J. Remote Sens. Soc. Jpn*, vol. 29, no. 1, pp. 216–225, 2009.

[11] D. J. Cavalieri, K. M. St. Germain, and C. T. Swift, "Reduction of weather effects in the calculation of sea-ice concentration with the DMSP SSM/I," *J. Glaciol.*, vol. 41, no. 139, pp. 455–464, 1995, doi: 10.3198/1995JoG41-139-455-464.

[12] D. J. Cavalieri, C. L. Parkinson, P. Gloersen, J. C. Comiso, and H. J. Zwally, "Deriving long-term time series of sea ice cover from satellite passive-microwave multisensor data sets," *J. Geophys. Res.*, vol. 104, no. C7, pp. 15803–15814, 1999, doi: 10.1029/1999JC900081.

[13] W. N. Meier, S. J. S. Khalsa, and M. H. Savoie, "Intersensor calibration between F-13 SSM/I and F-17 SSMIS near-real-time sea ice estimates," *IEEE Trans. Geosci. Remote Sens.*, vol. 49, no. 9, pp. 3343–3349, Sep. 2011.

[14] D. J. Cavalieri, C. L. Parkinson, N. DiGirolamo, and A. Ivanoff, "Intersensor calibration between F13 SSMIS and F17 SSMIS for global sea ice data records," *IEEE Geosci. Remote Sens. Lett.*, vol. 9, no. 2, pp. 233–236, 2012, doi: 10.1109/LGRS.2011.2166754.

[15] D. J. Cavalieri, P. Gloersen, and W. J. Campbell, "Determination of sea ice parameters with the NIMBUS 7 SMMR," *J. Geophys. Res.*, vol. 89, no. D4, pp. 5355–5369, 1984, doi: 10.1029/JD089iD04p05355.

Walter N. Meier was born in Farmington, MI, USA. He received the B.S. degree in aerospace engineering from the University of Michigan, Ann Arbor, MI, USA, in 1991, and the M.S. and Ph.D. degrees in aerospace engineering sciences from the University of Colorado, Boulder, CO, USA, within the university's interdisciplinary program in atmospheric and oceanic sciences, in 1992 and 1998, respectively.

He is currently a Research Scientist at the NASA Goddard Space Flight Center Cryospheric Sciences Laboratory, Greenbelt, MD, USA. Previously, he worked as Research Scientist at the National Snow and Ice Data Center, Boulder, CO, as an Adjunct Assistant Professor at the United States Naval Academy in Annapolis, MD, and as a Visiting Scientist at the United States National Ice Center in Washington, DC.

Dr. Meier is a member of the American Geophysical Union.

Alvaro Ivanoff received the B.Sc. degree in physics from the University of Toronto, Toronto, ON, Canada, in 1997.

He is currently with the NASA Goddard Space Flight Center Cryospheric Sciences Laboratory, Greenbelt, MD, USA, and ADNET Systems, Inc., Bethesda, MD.